Physica B 592 (2020) 412279

Contents lists available at ScienceDirect

Physica B: Physics of Condensed Matter

journal homepage: www.elsevier.com/locate/physb

Magneto-optical absorption in Pöschl–Teller-like quantum well

P.T.T. Le [a,b], Pham T. Vinh [c], Le T.N. Tu [c], Huynh V. Phuc [c], Chuong V. Nguyen [d], Nguyen N. Hieu [e,f], Le T. Hoa [e,f,*]

[a] Laboratory of Magnetism and Magnetic Materials, Advanced Institute of Materials Science, Ton Duc Thang University, Ho Chi Minh City 758307, Viet Nam
[b] Faculty of Applied Sciences, Ton Duc Thang University, Ho Chi Minh City 758307, Viet Nam
[c] Division of Theoretical Physics, Dong Thap University, Cao Lanh 870000, Viet Nam
[d] Department of Materials Science and Engineering, Le Quy Don Technical University, Ha Noi 100000, Viet Nam
[e] Institute of Research and Development, Duy Tan University, Da Nang 550000, Viet Nam
[f] Faculty of Natural Sciences, Duy Tan University, Da Nang 550000, Viet Nam

ARTICLE INFO

Keywords:
Magneto-optical properties
Transport properties
Pöschl–Teller-like quantum well

ABSTRACT

We study the magneto-optical properties of a Pöschl–Teller-like quantum well made of different materials such as GaAs, GaSb, InAs, and InSb. The energy difference becomes smaller with the wider well-width and becomes bigger with the deeper well-depth. The energy difference appears smallest in GaAs, followed by that in GaSb, while InSb shows the largest. The magneto-optical absorption coefficient (MOAC) shifts to the lower (higher) energy side when the well-width (well-depth and magnetic field) increases, but does not change the position with the change of temperature. The full-width at half-maximum (FWHM) increases with the increase of the well-depth, the temperature, and the magnetic field but decreases with the well-width. The phonon-emission process always happens stronger than the absorption one. The MOAC intensity in GaAs is the highest. The temperature-dependent-FWHM is supported by experimental results in GaAs quantum well.

1. Introduction

The magneto-optical absorption is one of the most attractive subjects since it strongly depends on the materials' electronic structure [1], and therefore, it has been vastly studied in recent decades. When studying the optical absorption of a doped parabolic quantum well (QW), Brey et al. [2] found that the number of electrons in QW have no effect on the absorption spectrum in parabolic QW. A similar result has been found in an asymmetric parabolic quantum dot [3], where the fact that the independence of the resonant frequency with the number of electrons in quantum dots has been demonstrated by experiment [4]. Rogers et al. [5] experimentally studied the photoconductivity in the presence of the magnetic field to infer the band parameters of QWs. The results showed that the exciton binding energy can be determined from linear extrapolation and having the values from 16 – 9 meV for well-widths from 2.2 to 11 nm. These values are slightly higher than those deduced from low-field measurements. In another experimental work, using magneto-transport and magneto-optics, Plaut et al. [6] found that mobility increases with the decrease of the electron concentration. The magneto-optical absorption has also been investigated in the Pöschl–Teller family [7,8], but it is still limited.

Because of its adjustable asymmetric property, the Pöschl–Teller potential [9] is anticipated to yield interesting optical properties [10–12], and therefore, this type of potential has attracted interest of many researchers. It is noted that there are rich types of Pöschl–Teller potential such as (Sec, Csc)-squared shape [10,11,13], Sech-squared shape [14–17], Cot-squared shape [18,19], Tan-squared shape [20–22], and Morse quantum well [23]. The research results showed that the Pöschl–Teller potential has rich of applications in optical devices [14] or in resonance tunneling devices [15]. Dong and Lemus [16] suggested an efficient method to obtain the normalization constants of the wave function. For the optical properties, the total absorption peak in Pöschl–Teller is found to increase while the peak position gives a blue-shift when the well-parameter [11] or the pressure [17] increases. The refractive index [10], the second-harmonic generation, and the optical rectification [11] have also been observed to display a blue-shift behavior with the bigger well-parameters.

In this paper, we study the magneto-optical absorption in one type of the Pöschl–Teller family potential: Tan-squared shape [20–22] via calculating the optical absorption coefficient in the presence of the magnetic field, called magneto-optical absorption coefficient (MOAC) where the two-photon process has been taken into account. We employ the perturbation method [24] which has been used successfully to obtain the optical absorption coefficient in the bulk semiconductor. This method has also been used widely to obtain the MOAC in quantum

* Corresponding author at: Institute of Research and Development, Duy Tan University, Da Nang 550000, Viet Nam.
E-mail addresses: lethithuphuong@tdtu.edu.vn (P.T.T. Le), lethihoa8@duytan.edu.vn (L.T. Hoa).

https://doi.org/10.1016/j.physb.2020.412279
Received 18 March 2020; Received in revised form 8 April 2020; Accepted 18 May 2020
Available online 20 May 2020

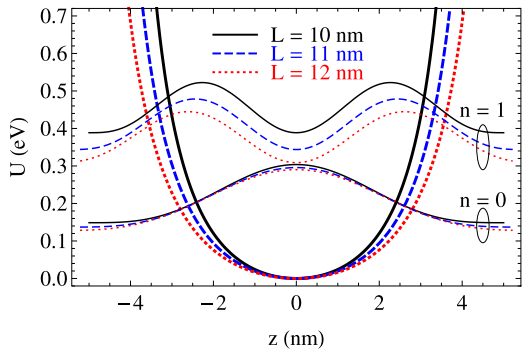

Fig. 1. The quantum well profiles and the probability density $|\xi(z)|^2$ for different well-widths at $U_0 = 0.228$ eV. The results are evaluated for GaAs material with $m_e = 0.067m_0$.

well [25], in graphene [26], and in some two-dimensional materials [27,28]. There are two benefits to this technique. Firstly, it allows to re-obtain previous results [29–33] in the one-photon absorption case. Secondly, it is much simpler than that based on Kubo formula [34,35]. The MOAC peaks are found to shift to the lower (higher) energy side when the well-width (well-depth) increases but does not change the position with the temperature. The FWHM, which is obtained by a computational method, increases proportionately with the well-depth and the temperature but decreases with the well-width. The phonon-emission process always happens stronger than the absorption one. Among the four materials: GaAs, GaSb, InAs, and InSb, the absorption happens strongest in GaAs. The T-dependent-FWHM in GaAs is observed to be consistent with the experimental result.

2. Basic formalism

The z-component of the effective-mass Hamiltonian for electrons in QW is

$$H_z = \frac{p_z^2}{2m_e} + U(z), \tag{1}$$

where $p_z = -i\hbar\partial/\partial z$ is the z-component of the momentum, m_e is the electron effective mass. Note that the electron effective mass is also dependent on the temperature [36–38]. However, the main purpose of this work is to study the MOAC due to the effect of the external field and the quantum-well characteristics. Therefore, we neglect the effect of the temperature on the electron effective mass in the present study. $U(z)$ is a potential belonging to the Pöschl–Teller family, which is given by [20–22]

$$U(z) = U_0 \tan^2\left(\frac{\pi z}{L}\right), \tag{2}$$

with U_0 and L being model parameters, called "well-depth" and "well-width", respectively. The envelope wave functions, $\xi_n(z)$, and eigenvalues, ε_n, are the solutions of the Schrödinger equation

$$H_z\xi_n(z) = \varepsilon_n\xi_n(z), \tag{3}$$

which are given by [16]

$$\xi_n(z) = A_n \cos^\gamma(\pi z/L) C_n^\gamma(\sin(\pi z/L)), \tag{4}$$

$$\varepsilon_n = (n+\gamma)^2 E_r, \tag{5}$$

where $n = 0, 1, 2, \ldots$, $C_n^\gamma(\pi z/L)$ are the Gegenbauer polynomials with $\gamma = (1+((E_r+4U_0)/E_r)^{1/2})/2$, and $E_r = \pi^2\hbar^2/(2m_eL^2)$. The normalization constant A_n is given as follows

$$A_n = \left(\frac{n!(n+\gamma)\Gamma^2(\gamma)}{\pi 2^{1-2\gamma}\Gamma(2\gamma+n)}\right)^{1/2}. \tag{6}$$

The quantum well profile shown in Eq. (2) and the probability density for the GaAs material is presented in Fig. 1.

When a uniform magnetic field $\mathbf{B} = (0, 0, B)$ is applied to the system, the Hamiltonian for the electrons is

$$H_e = \frac{\mathbf{P}^2}{2m_e} + U(z). \tag{7}$$

Here, $\mathbf{P} = \mathbf{p} + e\mathbf{A}$, $\mathbf{p} = (p_z, p_y, p_z)$, and $\mathbf{A}$ is the vector potential of the magnetic field, which is chosen as $\mathbf{A} = (0, Bx, 0)$. The full wave functions and eigenenergies of electrons are [29]

$$|\lambda\rangle = |N, n, k_y\rangle = \frac{e^{ik_y y}}{\sqrt{L_y}}\phi_N(x - x_0)\xi_n(z), \tag{8}$$

$$E_\lambda = E_{N,n} = \left(N + \frac{1}{2}\right)\hbar\omega_c + \varepsilon_n, \tag{9}$$

where the non-negative integer N denotes the Landau level (LL) index, $\omega_c = eB/m_e$ is the cyclotron frequency, and $\phi_N(x-x_0)$ is the normalized harmonic oscillator function centered at $x_0 = -\hbar k_y/(m_e\omega_c)$.

When an electromagnetic field (or radiation) of energy $\hbar\Omega$ is projected into the quantum well and the electrons in the system are assumed to interact with the phonon of energy $\hbar\omega_{\mathbf{q},\nu}$ and wave vector $\mathbf{q} = (q_\perp, q_z)$, the total Hamiltonian is

$$H = H_e + H_{ph} + H_{er} + H_{ep}, \tag{10}$$

where H_e is shown in Eq. (7). The Hamiltonian of phonon is

$$H_{ph} = \sum_{\mathbf{q},\nu}\hbar\omega_{\mathbf{q},\nu}d^\dagger_{\mathbf{q},\nu}d_{\mathbf{q},\nu}, \tag{11}$$

where $d^\dagger_{\mathbf{q},\nu}(d_{\mathbf{q},\nu})$ is the phonon creation (annihilation) operators, ν denotes the phonon branch index. The electron-radiation interaction Hamiltonian is [24]

$$H_{er} = -\frac{e}{m_e}(\mathbf{A}_{pt}\cdot\mathbf{P}), \tag{12}$$

where $\mathbf{A}_{pt}$ is the vector potential for the optical electric field. The electron–phonon interaction Hamiltonian is

$$H_{ep} = \sum_{\mathbf{q},\nu}V_{\mathbf{q},\nu}(e^{i\mathbf{q}\cdot\mathbf{r}}d^\dagger_{\mathbf{q}} + e^{-i\mathbf{q}\cdot\mathbf{r}}d_{\mathbf{q}}), \tag{13}$$

where $V_{\mathbf{q},\nu}$ is electron–phonon interaction strength.

3. Magneto-optical absorption coefficient

The expression of MOAC is expressed as follows for the ν-branch of phonon [24,27]

$$K^\nu = \frac{1}{N_\Omega V_0}\sum_{\lambda',\lambda}\mathcal{W}^{\pm,\nu}_{\lambda',\lambda}f_\lambda(1-f_{\lambda'}), \tag{14}$$

where N_Ω is the number photons, V_0 is the sample volume, $f_{\lambda\,(\lambda')}$ is the Fermi distribution function, and the transition matrix element caused by electron–photon–phonon interaction is given as follows [28,39–41]

$$\mathcal{W}^{\pm,\nu}_{\lambda',\lambda} = \frac{2\pi}{\hbar^3\Omega^2}\sum_{\lambda'',\mathbf{q}}\sum_{\ell=1}^{\infty}\left|\mathcal{M}^{\pm,\nu}_{\lambda',\lambda''}\right|^2\left|\mathcal{M}^{er}_{\lambda'',\lambda}\right|^2 \times\frac{(\alpha_0 q_\perp)^{2\ell}}{(\ell!)^2 2^{2\ell}}\delta(E_{\lambda'} - E_\lambda \pm \hbar\omega_{\mathbf{q},\nu} - \ell\hbar\Omega), \tag{15}$$

where α_0 is the dressing parameter, the plus (minus) sign corresponds to the phonon emission (absorption) process. Using Eq. (8), the matrix element for electron–photon interaction is found to be

$$\mathcal{M}^{er}_{\lambda'',\lambda} = \langle\lambda''|H_{er}|\lambda\rangle = -\frac{eA_0}{2m_e}\langle\lambda''|p_x|\lambda\rangle = -\frac{eA_0}{2m_e}B_{N'',N}\delta_{n'',n}\delta_{k''_y,k_y}, \tag{16}$$

where A_0 is amplitude of the vector $\mathbf{A}_{pt}$, and the dipole moment, $B_{N'',N} = \langle N''|p_x|N\rangle$, is

$$B_{N'',N} = \frac{i\hbar}{\alpha_c\sqrt{2}}(\sqrt{N+1}\delta_{N'',N+1} - \sqrt{N}\delta_{N'',N-1}), \tag{17}$$

with $\alpha_c = (\hbar/m_e\omega_c)^{1/2}$ being the cyclotron radius.

The matrix element for electron–phonon interaction, $\mathcal{M}^{\pm}_{\lambda',\lambda''}$, is [30]

$$\left|\mathcal{M}^{\pm,\nu}_{\lambda',\lambda''}\right|^2 = |\langle\lambda'|\mathcal{H}_{ep}|\lambda''\rangle|^2 = |V_{\mathbf{q},\nu}|^2|\mathcal{F}_{n',n''}(\pm q_z)|^2 \times \left|J_{N',N''}(q_\perp)\right|^2 N^{\pm}_{\mathbf{q},\nu}\delta_{k'_y,k''_y\mp q_y}, \quad (18)$$

where $N^{\pm}_{\mathbf{q},\nu} = N_{\mathbf{q},\nu} + 1/2 \pm 1/2$, with $N_{\mathbf{q},\nu}$ is the Bose distribution for phonon mode $(\mathbf{q},\nu)$, and

$$\mathcal{F}_{n',n''}(\pm q_z) = \int_0^\infty e^{\pm iq_z z}\xi^*_{n'}(z)\xi_{n''}(z)dz, \quad (19)$$

$$\left|J_{N',N''}(q_\perp)\right|^2 = \frac{k!}{(k+j)!}e^{-u}u^j[L^j_k(u)]^2, \quad (20)$$

with $u = \alpha_c^2 q_\perp^2/2$, $k = \min[N', N'']$, $j = |N'' - N'|$, and $L^j_k(u)$ being the associated Laguerre polynomials.

Using the above equations into Eq. (14) we obtain the expression for MOAC as follows

$$K^\nu = \sum_{N,n}\sum_{N',n'}\sum_{N'',n''} C(\lambda)\int_{-\infty}^{+\infty} dq_z|V_{\mathbf{q},\nu}|^2|\mathcal{F}_{n',n''}(\pm q_z)|^2 \times \int_0^{+\infty} dq_\perp q_\perp^3\left|J_{N',N''}(q_\perp)\right|^2\left\{N^{\pm}_{\mathbf{q},\nu}\delta(X^{\pm,\nu}_1) + \frac{\alpha_0^2 q_\perp^2}{16}N^{\pm}_{\mathbf{q},\nu}\delta(X^{\pm,\nu}_2)\right\}\delta_{n'',n}, \quad (21)$$

where the two-photon absorption process has been taken into account, and

$$C(\lambda) = \frac{e^2\hbar S^2|B_{N'',N}|^2\alpha_0^2}{8(2\pi\hbar\Omega)^3 n_r c\epsilon_0 m_e^2\alpha_c^4}f_{N,n}(1 - f_{N',n'}), \quad (22)$$

$$X^{\pm,\nu}_\ell = \Delta E \pm \hbar\omega_{\mathbf{q},\nu} - \ell\hbar\Omega, \ (\ell = 1, 2) \quad (23)$$

with $S = V_0/L$ being the normalization area, and

$$\Delta E = E_{N',n'} - E_{N,n} = (N' - N)\hbar\omega_c + \Delta\varepsilon_{n'n} \quad (24)$$

is the energy difference, with $\Delta\varepsilon_{n'n} = [(n' + \gamma)^2 - (n + \gamma)^2]\pi^2\hbar^2/(2m_eL^2)$ being the subband energy separation. The expression in Eq. (21) can be used to evaluate for different kinds of electron–phonon interaction.

For the longitudinal optical phonon ($\nu = LO$),

$$|V_{\mathbf{q},LO}|^2 = \frac{4\pi e^2\hbar\omega_0}{\epsilon_0\chi^* V_0 q_\perp^2}, \quad (25)$$

where $(\chi^*)^{-1} = (\chi_\infty)^{-1} - (\chi_0)^{-1}$ with χ_∞ (χ_0) being the high (static) frequency dielectric constants, $\hbar\omega_0$ is the optical phonon energy, and ϵ_0 refers to the permittivity of vacuum. Inserting Eq. (25) into Eq. (21) and making the calculation of integrals over q_z and $q_\perp$ we have

$$K^{LO} = \frac{4\pi e^2\hbar\omega_0}{\epsilon_0\chi^* V_0\alpha_c^2}\sum_{N,n}\sum_{N',n'}\sum_{N''} C(\lambda)I_{n',n}(P_1 + P_2), \quad (26)$$

where

$$I_{n',n} = \sum_{n''}\left(\int_{-\infty}^{+\infty}\left|\mathcal{F}_{n',n''}(\pm q_z)\right|^2 dq_z\right)\delta_{n'',n}, \quad (27)$$

which will be evaluated numerically, and

$$P_1 = N_0^-\delta(X_1^-) + N_0^+\delta(X_1^+), \quad (28)$$

$$P_2 = \frac{\alpha_0^2}{8\alpha_c^2}(N' + N'' + 1)\left[N_0^-\delta(X_2^-) + N_0^+\delta(X_2^+)\right], \quad (29)$$

where N_0 refers to $N_{\mathbf{q},\nu}$ for the electron–LO–phonon interaction. The Dirac δ-functions are replaced by Lorentzians of width $\Gamma^{\pm}_{N',N}$ [42]

$$\left(\Gamma^{\pm}_{N',N}\right)^2 = \sum_{\mathbf{q}}|\mathcal{M}^{\pm}_{\lambda',\lambda}|^2, \quad (30)$$

where $|\mathcal{M}^{\pm}_{\lambda',\lambda}|^2$ is presented in Eq. (18) where the index λ'' is replaced by λ.

Table 1
Parameters of the materials [43–45].

Parameters	GaAs	GaSb	InAs	InSb
m_e (m_0)	0.067	0.043	0.022	0.0116
n_r	3.2	3.8	3.51	4.0
χ_0	13.18	15.68	15.15	17.76
χ_∞	10.89	14.44	12.25	15.68
$\hbar\omega_0$ (meV)	36.25	28.8	29.6	23.6

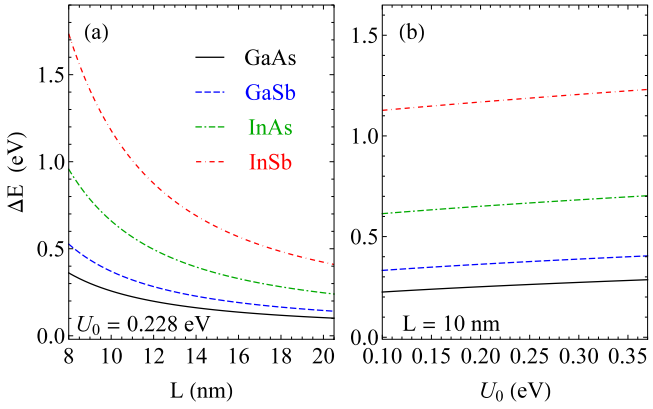

Fig. 2. The energy difference as a function of (a) L and (b) U_0 for different materials at $B = 10$ T.

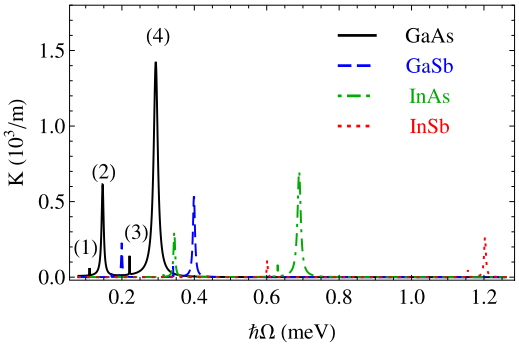

Fig. 3. The MOAC versus photon energy, $\hbar\Omega$, for different materials at $U_0 = 0.228$ eV, $B = 10$ T, $L = 10$ nm, and $T = 77$ K.

4. Results and discussion

In this section, the numerical results are evaluated for the electric quantum limit $n = 0, n' = 1$. The used parameters are shown in Table 1, the other parameters are $\alpha_0 = 7.5$ nm, and $n_e = 3\times10^{22}$ m^{-3} [19].

In Fig. 2, we show the dependence of ΔE on (a) L and (b) U_0 for different materials. The usual reduction of the energy separation with the "well-width", L, is observed in Fig. 2(a) for four materials, which can be explained from the relation $\Delta E \sim (1 + 2\gamma)\pi^2\hbar^2/(2m_eL^2)$. It is clear that ΔE decreases when L increases, being in agreement with previous work [19]. The increase of ΔE with an increase of U_0 is also observed in Fig. 2(b), agreeing with previous work [7]. Besides, with the biggest electron effective mass (see Table 1), GaAs displays the smallest ΔE, followed by that of GaSb, while InSb shows the largest. This is in agreement with previous work [8] and has a direct effect on the MOAC peak position as the following.

Fig. 3 depicts the MOAC as a function of photon energy in QW made of different materials. The results are analyzed only for the transition from $N = 0$ to $N' = 1$. There are four peaks in each curve which describe different transitions. The peak positions satisfy the condition

$$\ell\hbar\Omega = \Delta E \pm \hbar\omega_0, \ (\ell = 1, 2). \quad (31)$$

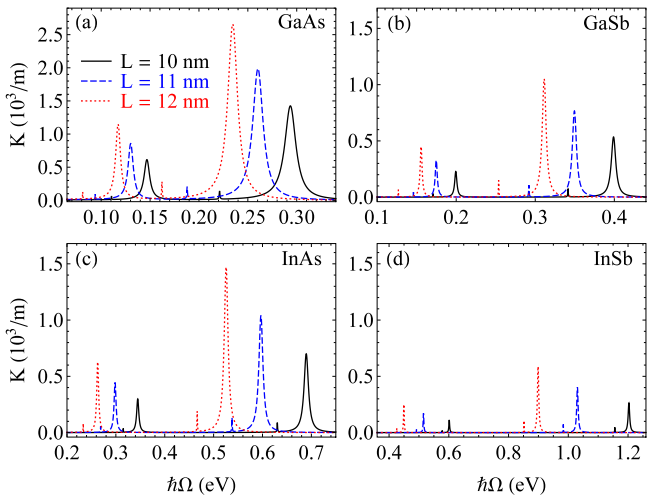

Fig. 4. The MOAC versus photon energy, $\hbar\Omega$, for different values of L. The results are evaluated in different materials at $U_0 = 0.228$ eV, $B = 10$ T, and $T = 77$ K. The panels (a), (b), (c), and (d) correspond to GaAs, GaSb, InAs, and InSb, respectively.

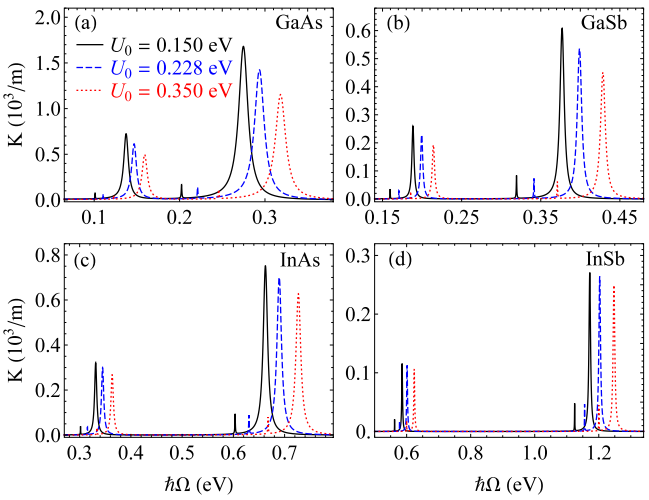

Fig. 6. The MOAC versus photon energy, $\hbar\Omega$, for different values of U_0. The results are evaluated in different materials at $L = 10$ nm, $B = 10$ T, and $T = 77$ K. The panels (a), (b), (c), and (d) correspond to GaAs, GaSb, InAs, and InSb, respectively.

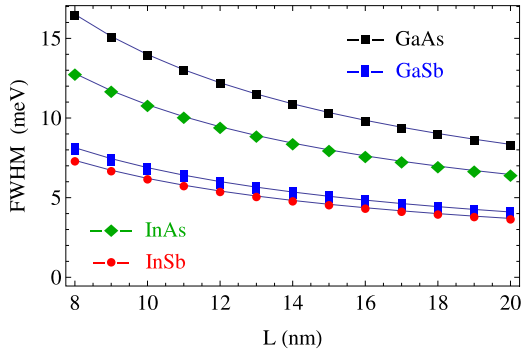

Fig. 5. The FWHM versus well-width in different materials. The results are evaluated for one-photon absorption and phonon emission processes at $U_0 = 0.228$ eV, $B = 10$ T, and $T = 77$ K.

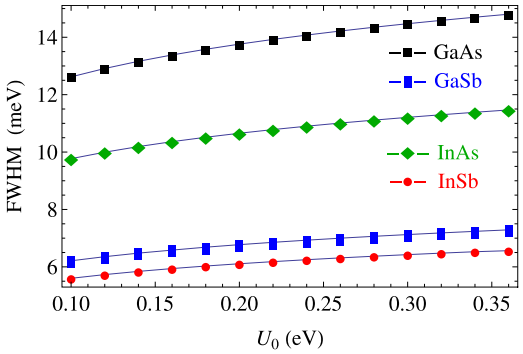

Fig. 7. The FWHM versus well-depth in different materials. The results are evaluated for one-photon absorption and phonon emission processes at $L = 10$ nm, $B = 10$ T, and $T = 77$ K.

In the case of GaAs, for example, the peaks labeled by (1) and (3) locate at $\hbar\Omega = 0.111$, and 0.222 eV, respectively, satisfying the condition (31) with $\ell = 2$. These two peaks display the two-photon absorption process simultaneous with the process of absorption and/or emission of one phonon. Meanwhile, the peaks labeled by (2) and (4) locate at $\hbar\Omega =$ 0.147 and 0.294 eV, which have the same meaning with the peaks (1) and (3) but for $\ell = 1$. Moreover, since the energy difference in GaAs is the smallest (see Fig. 2), the MOAC peaks in this material appear in the lowest region, while these in InSb locate in the highest one. Because the dielectric constants in InSb are the biggest, the MOAC intensities in this material are the lowest, followed by that in GaSb, while GaAs displays the highest. The result obtained here is in accordance with that available in Pöschl–Teller QW [8].

The effect of the well-width on MOAC for different materials is illustrated in Fig. 4. The main trend is that when the L-parameter increases the MOAC peaks in all four materials shift to the left-hand side (red-shift) and show an increase in the intensity as well. These results are in agreement with those in previous works [19,46]. The red-shift behavior is caused by the downsizing of the energy difference with the wider well-width (see Fig. 2(a)). The increase of the peak intensity is related to the decrease of the Lorentzian width, which has a closed relationship with the FWHM as investigated details in Fig. 5.

In Fig. 5, we display the FWHM as a function of the L-parameter at given other parameters. The results are evaluated only for the one-photon absorption and phonon emission process but the phenomenon can be also valid in other cases. We can see that the FWHM in all four materials shrinks with the expansion of the well-width. This signifies that the wider well-width is the weaker electron–phonon interaction is. This is in agreement with what happened in other quantum well shapes [25,47–49]. Besides, the FWHM in GaAs displays the highest, followed by that of InAs, and the InSb shows the smallest. This reveals that the electron–phonon interaction in GaAs is the strongest while that in InSb is the weakest among the four materials.

In Fig. 6, we depict the $\hbar\Omega$ dependence of the MOAC for different well-depths. With the increase of U_0-parameter, the absorption peaks shift to the higher energy side (blue-shift) and reduce their values. The blue-shift behavior is the direct consequence of the increase of the energy difference with the well-depth shown (see Fig. 2(b)), being in agreement with that in other type of the Pöschl–Teller potential family [7]. The reduction behavior of the absorption peaks means that the deeper well-depth is, the smaller the transition probability of electron is. Moreover, the MOAC intensity in GaAs are still the biggest, making it the best candidate for optoelectronics devices among the four materials.

The dependence on the well-depth of the FWHM is shown in Fig. 7. The FWHM is found to increase with U_0 in all four different materials, where the GaAs displays the highest and InSb shows the lowest. The enhance of the FWHM reveals that the electron–phonon scattering will be stronger if the well-depth becomes deeper.

In Fig. 8, we show the dependence of the MOAC on $\hbar\Omega$ for different temperatures at given values of L, B, and U_0. The results show

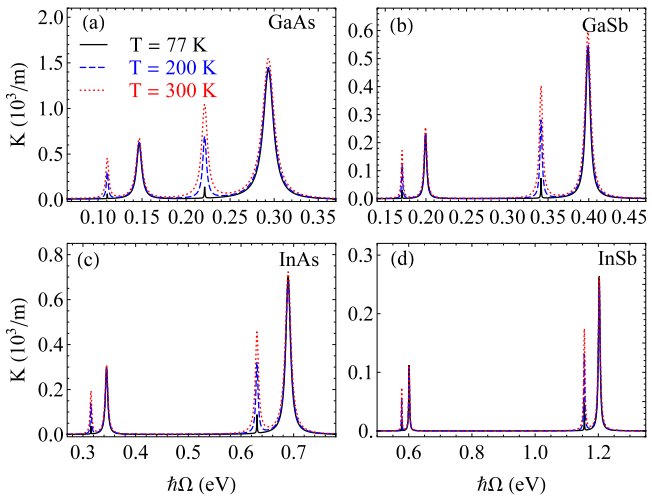

Fig. 8. The MOAC versus photon energy, $\hbar\Omega$, for different values of temperature. The results are evaluated in different materials at $L = 10$ nm, $B = 10$ T, and $U_0 = 0.228$ eV. The panels (a), (b), (c), and (d) correspond to GaAs, GaSb, InAs, and InSb, respectively.

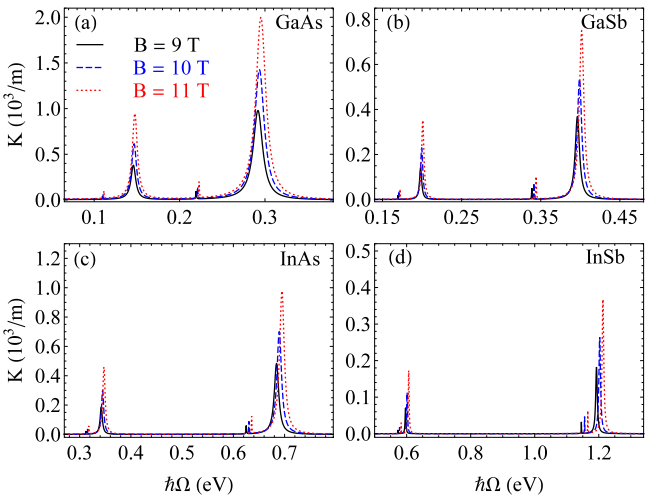

Fig. 10. The MOAC versus photon energy, $\hbar\Omega$, for different values of B. The results are evaluated in different materials at $L = 10$ nm, $U_0 = 0.228$ eV, and $T = 77$ K. The panels (a), (b), (c), and (d) correspond to GaAs, GaSb, InAs, and InSb, respectively.

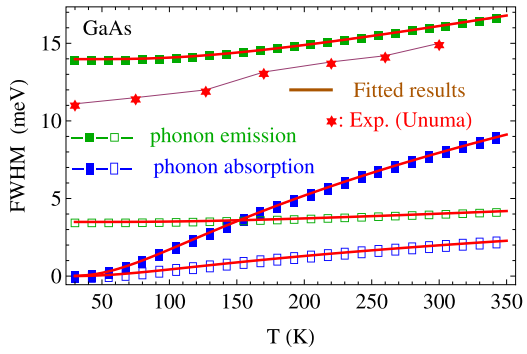

Fig. 9. The FWHM in GaAs versus temperature at $L = 10$ nm, $B = 10$ T, and $U_0 = 0.228$ eV. The filled and empty symbols, respectively, refer to the one- and two-photon processes. Red asterisk dots present the experimental data in Ref. [50,51].

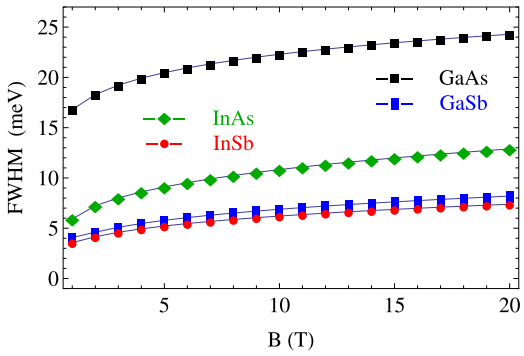

Fig. 11. The FWHM versus magnetic field in different materials. The results are evaluated for one-photon absorption and phonon emission processes at $L = 10$ nm, $U_0 = 0.228$ eV, and $T = 77$ K.

that when the temperature increases, the MOAC peaks do not change their positions but increase their intensities, agreement with previous works [7,8,19]. Moreover, the temperature has a significant effect on the intensity of phonon absorption peaks (the first and third peaks from the left to right in each panel of Fig. 8) rather than the emission phonon peaks (the second and fourth peaks). For the FWHM, another important feature of the absorption peak, the increasing temperature leads to the broadening in the peak shapes in both phonon absorption and emission processes. This will be discussed in detail in Fig. 9.

The temperature-dependent-FWHM is presented in Fig. 9 for all four possible processes in GaAs material. We can see that (1) the FWHM due to the one-photon process is always wider than that due to the two-photon; (2) with the increase of T, the FWHM caused by the phonon-absorption grows more rapidly, but never reach the value of FWHM due to the phonon-emission one. It is shown that the phonon-emission process is superior to the phonon-absorption one. This is in agreement with previous work [52], where the authors claimed that the electrons, whose energies are bigger than optical phonon energy, are mainly scattered by a phonon-emission process.

We also show here the experimental data, which is illustrated by the red asterisk dots in Fig. 9. These experimental data are adapted from previous reports in single GaAs squared quantum wells [50,51]. We can see that the increased law of the FWHM by phonon-emission is in good agreement with the experimental result of Unuma et al.

In Fig. 10, we show the magnetic field effect on the absorption spectrum in four different materials. When the magnetic field increases, the MOAC peaks shift to the higher energies region (blue-shift) and reduce their intensities. The blue-shift behavior is the result of the increase of the energy difference, ΔE, agreeing with previous work [22], while the reduction of intensity is explained by the decrease of the magnetic length, α_c. It is clear from Eq. (26) that K^{LO} is proportional to $\alpha_c^{-6} \sim B^3$. This relation illustrates clearly the increase of the MOAC with the increase of the magnetic field in all four materials.

Finally, the effect of the magnetic field on the FWHM is presented in Fig. 11. The FWHM is found to increase when the magnetic field increases in all four materials, agreeing with previous works [25]. Besides, the FWHM in GaAs is found to be the largest, followed by that of InAs, while the FWHM in InSb is the smallest. This means that the electron–LO–phonon interaction in GaAs is the strongest, making this material advantage in optical and optical–electronic applications in comparison to the other materials.

5. Summary and conclusion

We have studied the effect of quantum well's characteristics and the temperature on the magneto-optical properties of a Pöschl–Teller-type QW. The results are evaluated for four different materials: GaAs, GaSb, InAs, and InSb. The energy different decreases with increasing well-width but increases with increasing well-depth. Among given materials, GaAs shows the smallest ΔE, followed by that of GaSb, while InSb witness the largest. The MOAC is found (i) to shift to

the lower (higher) energy side when the well-width (well-depth and magnetic field) increases, but (ii) to maintain its position with the change of temperature. The FWHM increases with the increase of the well-depth, the magnetic field, and the temperature but decreases with the well-width. The phonon-emission process is always superior to the phonon-absorption one. The absorption process in GaAs always happens strongest, this makes GaAs the best candidate, in comparison to the others, for optoelectronic devices.

CRediT authorship contribution statement

P.T.T. Le: Investigation, Validation. **Pham T. Vinh:** Investigation, Validation. **Le T.N. Tu:** Investigation, Validation. **Huynh V. Phuc:** Investigation, Writing - original draft, Writing - review & editing. **Chuong V. Nguyen:** Conceptualization, Investigation, Validation. **Nguyen N. Hieu:** Investigation, Validation, Funding acquisition, Writing - original draft. **Le T. Hoa:** Investigation, Writing - original draft, Writing - review & editing.

Declaration of competing interest

The authors declare that they have no known competing financial interests or personal relationships that could have appeared to influence the work reported in this paper.

Acknowledgment

This research is supported by the project SPD2019.01.15.

References

[1] J.L. Menéndez, B. Bescós, G. Armelles, R. Serna, J. Gonzalo, R. Doole, A.K. Petford-Long, M.I. Alonso, Phys. Rev. B 65 (2002) 205413.
[2] L. Brey, N.F. Johnson, B.I. Halperin, Phys. Rev. B 40 (1989) 10647(R).
[3] F.M. Peeters, Phys. Rev. B 42 (1990) 1486(R).
[4] C. Sikorski, U. Merkt, Phys. Rev. Lett. 62 (1989) 2164.
[5] D.C. Rogers, J. Singleton, R.J. Nicholas, C.T. Foxon, K. Woodbridge, Phys. Rev. B 34 (1986) 4002.
[6] A.S. Plaut, I.V. Kukushkin, K.v. Klitzing, K. Ploog, Phys. Rev. B 42 (1990) 5744.
[7] K.D. Pham, L. Dinh, C.V. Nguyen, N.N. Hieu, P.T. Vinh, L.T.N. Tu, H.V. Phuc, Appl. Phys. A 125 (2019) 166.
[8] K.D. Pham, L.V. Tung, D.V. Thuan, C.V. Nguyen, N.N. Hieu, H.V. Phuc, J. Appl. Phys. 126 (2019) 124301.
[9] G. Pöschl, E. Teller, Z. Phys. 83 (1933) 143.
[10] H. Yildirim, M. Tomak, J. Appl. Phys. 99 (2018) 093103.
[11] H. Yıldırım, M. Tomak, Phys. Rev. B 72 (2005) 115340.
[12] S. Sakiroglu, F. Ungan, U. Yesilgul, M. Mora-Ramos, C. Duque, E. Kasapoglu, H. Sari, I. Sokmen, Phys. Lett. A 376 (2012) 1875.
[13] H. Yıldırım, M. Tomak, Phys. Status Solidi b 243 (2006) 4057.
[14] B.Y. Tong, Solid State Commun. 104 (1997) 679.
[15] B.Y. Tong, N. Kiriushcheva, Phys. Lett. A 229 (1997) 49.
[16] S.H. Dong, R. Lemus, Int. J. Quantum Chem. 86 (2002) 265.
[17] V.U. Unal, E. Aksahin, O. Aytekin, Physica E 47 (2013) 103.
[18] I.I. Gol'dman, V.D. Krivchenkov, V.I. Kogan, V.M. Galitskii, Problems in Quantum Mechanics, Inforsearch, London, 1960.
[19] K.D. Pham, N.N. Hieu, L.T.T. Phuong, B.D. Hoi, C.V. Nguyen, H.V. Phuc, Appl. Phys. A 124 (2018) 656.
[20] F. Gori, L. d. l. Torre, Eur. J. Phys. 24 (2003) 1.
[21] S. Flügge, Practical Quantum Mechanics, Springer-Verlag, Berlin, 1971.
[22] F. Ungan, S. Pal, M.E. Mora-Ramos, J.C. Martínez-Orozco, Optik 188 (2019) 12.
[23] F. Ungan, S. Pal, M.K. Bahar, M.E. Mora-Ramos, Physica E 113 (2019) 86.
[24] S.L. Chuang, Physics of Optoelectronic Devices, Wiley, New York, 1995.
[25] L.V. Tung, P.T. Vinh, H.V. Phuc, Physica B 539 (2018) 117.
[26] H.V. Phuc, N.N. Hieu, Opt. Commun. 344 (2015) 12.
[27] C.V. Nguyen, N.N. Hieu, N.A. Poklonski, V.V. Ilyasov, L. Dinh, T.C. Phong, L.V. Tung, H.V. Phuc, Phys. Rev. B 96 (2017) 125411.
[28] N.D. Hien, C.V. Nguyen, N.N. Hieu, S.S. Kubakaddi, C.A. Duque, M.E. Mora-Ramos, L. Dinh, T.N. Bich, H.V. Phuc, Phys. Rev. B 101 (2020) 045424.
[29] J.S. Bhat, B.G. Mulimani, S.S. Kubakaddi, Phys. Rev. B 49 (1994) 16459.
[30] J.S. Bhat, S.S. Kubakaddi, B.G. Mulimani, J. Appl. Phys. 70 (1991) 2216.
[31] H.J.G. Meyer, Phys. Rev. 112 (1958) 298.
[32] E.R. Generazio, H.N. Spector, Phys. Rev. B 20 (1979) 5162.
[33] C.T. Giner, M. Antón, Phys. Status Solidi b 133 (2) (1986) 563.
[34] M. Singh, B. Tanatar, Phys. Rev. B 41 (1990) 12781.
[35] B. Tanatar, M. Singh, Phys. Rev. B 42 (1990) 3077.
[36] H.M. Baghramyan, M.G. Barseghyan, A.A. Kirakosyan, R.L. Restrepo, C.A. Duque, J. Lumin. 134 (2013) 594.
[37] I.A. Yugova, A. Greilich, D.R. Yakovlev, A.A. Kiselev, M. Bayer, V.V. Petrov, Y.K. Dolgikh, D. Reuter, A.D. Wieck, Phys. Rev. B 75 (2007) 245302.
[38] E. Reyes-Gómez, N. Raigoza, L.E. Oliveira, Phys. Rev. B 77 (2008) 115308.
[39] W. Xu, R.A. Lewis, P.M. Koenraad, C.J.G.M. Langerak, J. Phys.: Condens. Matter. 16 (2004) 89.
[40] W. Xu, Phys. Rev. B 57 (1998) 12939.
[41] K. Seeger, Semiconductor Physics: An Introduction, Vol. 40, Springer-Verlag, Berlin Heidelberg, 1985.
[42] M.P. Chaubey, C.M. Van Vliet, Phys. Rev. B 33 (1986) 5617.
[43] S. Adachi, J. Appl. Phys. 58 (1985) R1.
[44] E. Li, Physica E 5 (2000) 215.
[45] P.P. Paskov, J. Appl. Phys. 81 (1997) 1890.
[46] K.D. Pham, L. Dinh, P.T. Vinh, C.A. Duque, H.V. Phuc, C.V. Nguyen, Superlattices Microstruct. 120 (2018) 738.
[47] H.V. Phuc, L. Dinh, T.C. Phong, Superlattices Microstruct. 59 (2013) 77.
[48] H.V. Phuc, N.D. Hien, L. Dinh, T.C. Phong, Superlattices Microstruct. 94 (2016) 51.
[49] H.V. Phuc, N.T.T. Thao, L. Dinh, T.C. Phong, J. Phys. Chem. Solids 75 (2014) 300.
[50] T. Unuma, T. Takahashi, T. Noda, M. Yoshita, H. Sakaki, M. Baba, H. Akiyama, Appl. Phys. Lett. 78 (2001) 3448.
[51] T. Unuma, M. Yoshita, T. Noda, H. Sakaki, H. Akiyama, J. Appl. Phys. 93 (2003) 1586.
[52] S.-H. Park, D. Ahn, E.H. Park, T.K. Yoo, Y.-T. Lee, Appl. Phys. Lett. 87 (2005) 044103.